Electronic supplementary information (ESI)

Ordered Gyroidal Tantalum Oxide Photocatalysts: Eliminating Diffusion Limitations and Tuning Surface Barriers

Alexey S. Cherevan,[a] Spencer Robbins,[b] Dennis Dieterle,[a] Paul Gebhardt,[a] Ulrich Wiesner,[b] and Dominik Eder*[a]

[a] Institut für Materialchemie, Technische Universität Wien, Getreidemarkt 9/BC/2, A-1060, Vienna, Austria

[b] Department of Materials Science and Engineering, 330 Bard Hall, Cornell University, Ithaca, NY 14853, USA
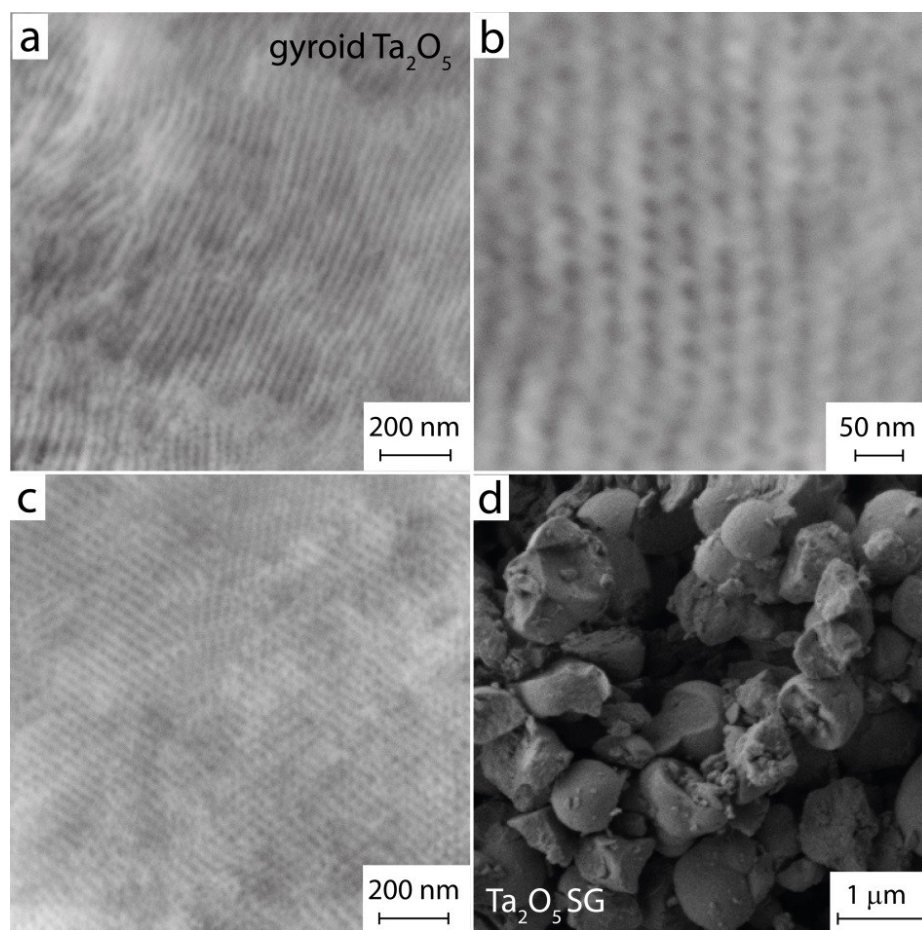
Supplementary figures

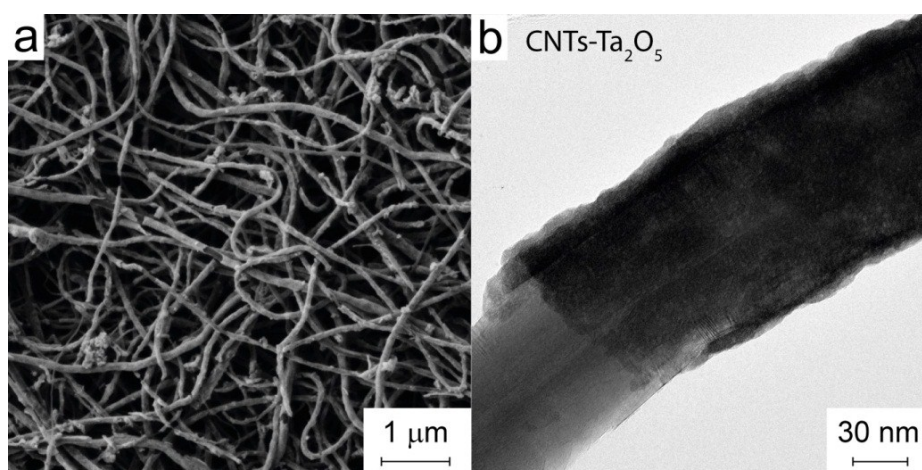**Figure S1.** (a-c) SEM images of the gyroid Ta_2O_5 and (d) reference Ta_2O_5 SG powder.

Figure S2. (a) SEM and (b) TEM images of the CNT-Ta_2O_5 hybrid before the template removal.
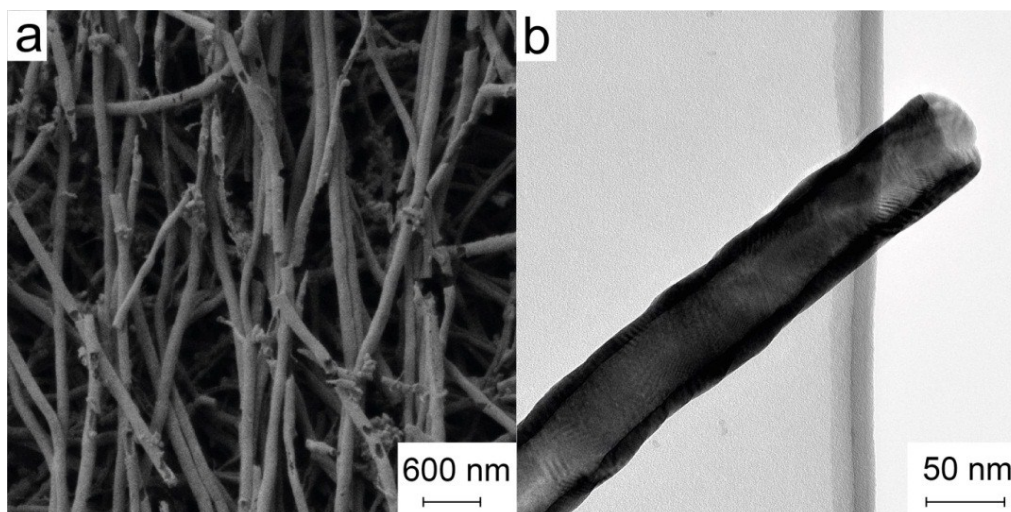
Figure S3. (a) SEM and (b) TEM images of the Ta_2O_5 NTs demonstrating complete removal of the CNT templates and the presence of tubular morphology of the structures.
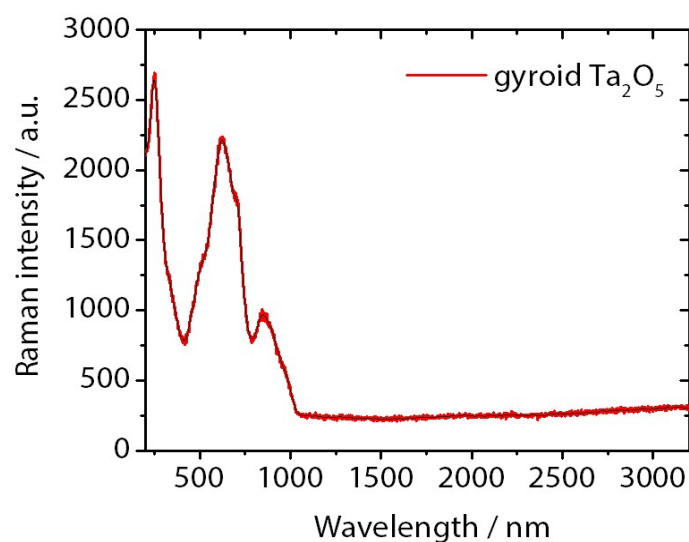

Figure S4. Extended Raman spectrum of the gyroid Ta_2O_5, showing the typical peaks for β-Ta_2O_5 and confirming the absence of any carbon-related peaks.

Stability

In order to verify stability of the mesoporous matrix towards harsh conditions of the water splitting experiment (UV and ultrasound-assisted treatments), the sample after the water splitting experiment was investigated by means of HRTEM. The micrographs in Figure S4 reveal that the mesoporous structure of the oxide is well preserved confirming good stability towards H_2 production during the water splitting experiment.
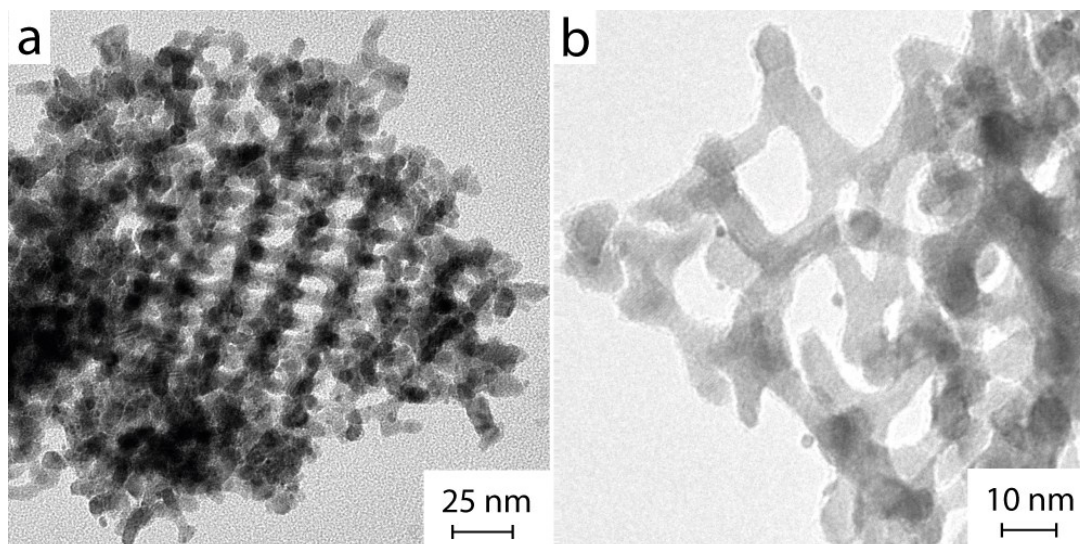
Figure S5. TEM images of the gyroid Ta_2O_5 after water splitting experiment demonstrating preserved mesoporous of gyroid architecture.

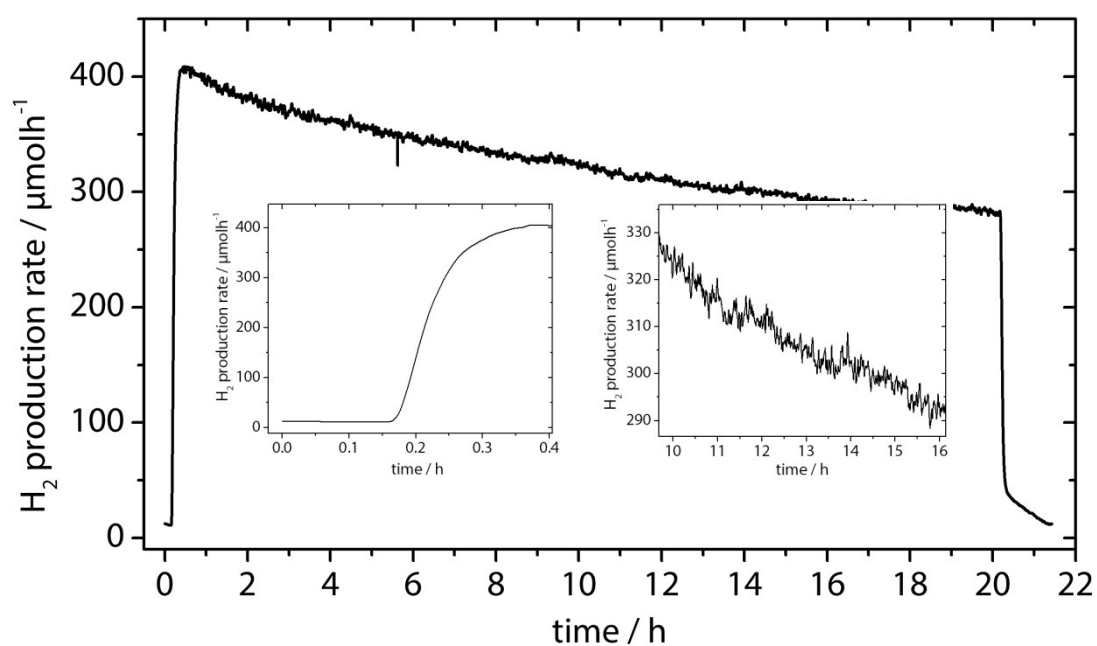**Figure S6.** H_2 evolution rate plotted against time for the 20 h water splitting run performed with 15 mg of the for the gyroid Ta_2O_5 photocatalyst powder. Deactivation reaches around 25 % after the experimental time. The slope, however, levels off with time indicating that stable evolution level of around 250 µmol/h (corresponding to 16.7 $mmolh^{-1}g^{-1}$) can be reached at long experimental times.

Characterization methods

The ISO/Ta_2O_5 hybrid **SAXS** pattern was obtained at the G1 station of the Cornell High Energy Synchrotron Source (CHESS) with beam energy of 10.7 keV. The mesoporous crystalline Ta_2O_5 SAXS pattern was obtained on a home-built beamline with a phosphor-coupled CCD detection as previously described.[1]

SEM images were acquired using Zeiss XB 1540 EsB scanning electron microscope to obtain visual information on the long range pore order and morphology of the samples. Typically acceleration voltage of 2 keV and secondary electron detection mode were used.

TEM images were obtained using FEI Tecnai F20 transmission electron microscope equipped with a field emission gun in bright field mode using 200 keV acceleration voltage. The sample was prepared from a suspension in ethanol without ultrasonication, using a copper Lacey carbon coated grids (Plano, 200 mesh).

XRD was performed using Bruker D8 Advance machine with Bragg-Brentano geometry equipped with a Ni filter and a Lynxeye super speed detector using a Cu K_α irradiation with λ_1 of 1.540596 Å and λ_2 of 1.544410 Å with the ratio of 0.442227. The average crystallite size was calculated using Scherrer equation[2] and a shape factor of 0.9.[3]

Diffuse reflectance spectra were recorded in UV-vis region using Jasco V-670 UV-VIS-NIR photo spectrometer by means of a diffuse reflectance unit containing an Ulbricht-sphere. Samples were fixed in a micro sample holder with diameter of 3 mm.

Raman spectra were obtained using Jobin Yvon Horiba LABRAM HR dispersive Raman spectrometer equipped with a CCD detector, a Nd:Yag-Laser (λ = 532 nm) and an Olympus BX41 optical microscope.

N_2 physisorption measurements were performed with a Micromeritics ASAP 2020 surface area and porosity analyzer. The powdered samples were degassed at 120 °C under vacuum for at least 6 h prior to measurements. Surface areas were determined according to Brunauer-Emmett-Teller (**BET**)[4] and pore size distributions were calculated according to the Barrett-Joyner-Halenda (**BJH**)[5].

EIS measurements were conducted in a three electrode electrochemical cell made of Teflon. A platinum wire was used as a counter electrode, Ag/AgCl as a reference electrode (both from CH Instruments) and 1M K_2SO_4 as the electrolyte. FTO conductive glass (Sigma Aldrich, 7 Ω/cm) was first cut into 1x1 cm^2 pieces and cleaned through consecutive sonication in acetone and ethanol for 5 min. The samples were dispersed in ethanol, drop-casted onto an FTO piece, dried overnight at 60 °C and calcined in air at 350 °C for 30 min (2 K/min).
Prior to the EIS measurement, nitrogen gas was purged through the electrolyte solution for 10 min. The data were collected using a Metrohm PGSTAT302N equipped with a FRA32M module and an Autolab Optical bench electrochemical workstation (Deutsche Metrohm GmbH) controlled by NOVA software (v1.10.3). EIS was performed using an AC voltage of 10 mV and within a frequency range of 0.1 to 100000 Hz. Mott-Schottky plots were obtained though variation of the DC voltage from 0.5 to -0.5 V vs Ag/AgCl with 0.05 V step size. The

respective values of the flat band potentials, V_{fb}, were obtained from the intercept of the curves with the x-axis of the Mott-Schottky plots.

Calculation of the **apparent quantum yields** (AQY) of the photocatalytic reaction has been performed based on the following equation:

$$AQY\ (\%) = \frac{\#\ of\ H_2\ molecules\ produced \times 2}{\#\ of\ incident\ light\ photons} \times 100.$$

Number of H_2 molecules has been derived from the activity value as follows:

$$\#\ of\ H_2\ molecules\ produced\ per\ second = \frac{activity\ (\mu mol/h) \times N_A\ (molecules/mol)}{3600\ (s/h) \times 1000000 (\mu mol/mol)}$$

Number of incident photons has been calculated using power energy meter PM100D (Thorlabs) according to the scheme in Figure S6. To estimate the number of photons absorbed by the photocatalyst particles we first (Figure S6a) measured intensity of light that reach the detector after passing through the reactor filled with pure reaction solution($W_{solution}$), and then (Figure S6b) measured intensity of light that reach the detector after passing through the reactor filled with sample dispersed within the solution ($W_{solution+sample}$). The difference between the values (ΔW) indicated amount of light that has been trapped by the suspended photocatalyst particles. We further considered specifications of the lamp (e.g. spatial light distribution) as well as reactor geometry to integrate total amount of light absorbed by the photocatalyst during the experiment.
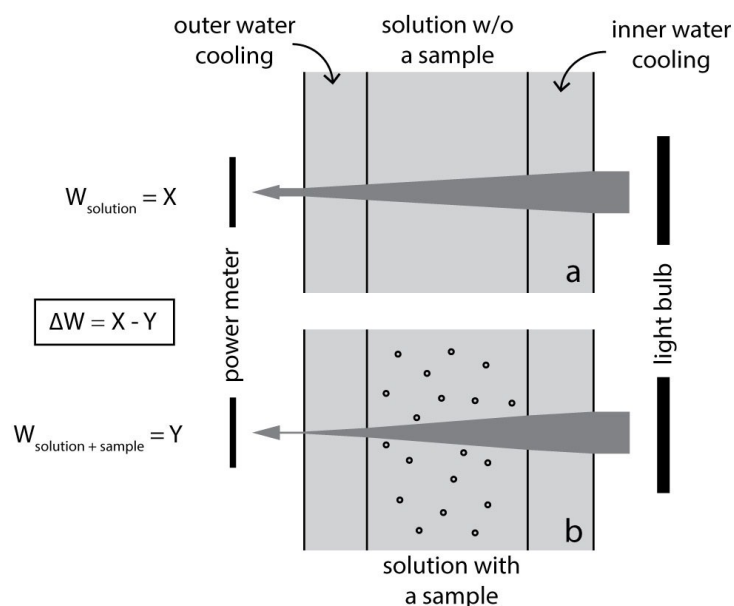

Figure S7. Calculation of the principle of the amount of absorbed light calculation: The value ΔW was estimated as a difference between two measurements, a and b.

The value of light power (measured in J/s=W) can then be related to a number of photons if one knows the energy of a single photon E_{ph} defined by the following expression:

$$E_{ph}(J) = h\nu = \frac{h(J \times s) \times c(m/s)}{\lambda(m)}$$

Further considering spectral distribution of the lamp and the fact that only photons with wavelength below 330 nm can potentially be absorbed by the Ta_2O_5 (see Figure 2f), number of useful photons that have been absorbed by the photocatalyst can be calculated as follows:

$$\# \ of \ incident \ light \ photons = \frac{\Delta W \ (J/s) \times 3600(sec/h)}{E_{ph \ average}(J)}$$

The calculation simplifies the procedure of AQY calculation by substituting integration to a less precise averaging to calculate the photon energy. This, however, results in a maximum error of around 5 %.

AQYs for all Ta_2O_5 samples have been evaluated using the procedure described above. Summary of the calculation is presented in Table S1.

Table S1. Calculated AQY values in sacrificial water splitting towards H_2 evolution for the tested Ta_2O_5 samples.

Sample	H_2 production level / μmol h^{-1}	AQY / %
Ta_2O_5 SG	78	0.30
gyroid Ta_2O_5	955/1188	3.73/4.64
Ta_2O_5 NTs	262	1.02

Bibliography

1 A. C. Finnefrock, R. Ulrich, G. E. S. Toombes, S. M. Gruner and U. Wiesner, *J. Am. Chem. Soc.*, 2003, **125**, 13084–13093.
2 A. L. Patterson, *Phys. Rev.*, 1939, **56**, 978–982.
3 U. Holzwarth and N. Gibson, *Nat. Nanotechnol.*, 2011, **6**, 534–534.
4 S. Brunauer, P. H. Emmett and E. Teller, *J. Am. Chem. Soc.*, 1938, **60**, 309–319.
5 E. P. Barrett, L. G. Joyner and P. P. Halenda, *J. Am. Chem. Soc.*, 1951, **73**, 373–380.